CF_2Cl_2, $CFCl_3$, and odd chlorine. Transport was treated by using the expedient concept of eddy diffusion. Diffusion coefficients were taken from (8) but were adjusted upward by a factor of 2 between 16 and 20 km in order to improve the agreement with observational data for NO. The chemical model combined lists of reactions given in (4) and (8).
17. The lifetime is obtained by dividing the total quantity of atmospheric Freon by its corresponding production or destruction rate under steady-state conditions.
18. A discussion of possible biological effects is given in K. Smith *et al.*, *Biological Impacts of Increased Intensities of Solar Ultraviolet Radiation* (National Academy of Sciences, Washington, D.C., 1973). We should caution that the papers which have appeared to date discussing Freon and its effects on ozone, including the present contribution, are preliminary in nature. They do not establish that the effects discussed here will necessarily ensue from continued Freon usage. They develop a case, however, for serious concern and emphasize the need for intensive further investigation. We have not explicitly allowed for possible removal of stratospheric chlorine by heterogeneous reactions, and we have assumed that the Freon lifetime is set by photolysis. If additional removal processes could be identified for Freon, or if additional sinks could be identified for stratospheric odd chlorine, the atmospheric and biological impacts of Freon would be reduced accordingly.
19. J. E. Lovelock, *Nature (Lond.)* **252**, 292 (1974).
20. C. B. Farmer, *Can. J. Chem.* **52**, 1544 (1974).
21. We acknowledge valuable discussions with M. Molina, F. S. Rowland, and R. L. McCarthy during preparation of this manuscript. Supported by NSF grant GA-33990X and NASA grant NG 2031.

29 September 1974; revised 8 November 1974

Earthquake Prediction: Modeling the Anomalous V_P/V_S Source Region

Abstract. *Soviet observations of anomalously low values of the ratio of the compressional wave velocity to the shear wave velocity (V_P/V_S) in a restricted volume around the locus of a future earthquake are duplicated by models based on the dilatancy hypothesis. In nature the cracks that cause the dilation may be oriented, leading to anisotropic seismic wave propagation in the anomalous region. The models show that vertical cracks are most effective in producing the observed effects, but that a slightly higher density of randomly oriented cracks will yield similar effects. The premonitory observations at Blue Mountain Lake, New York, are also duplicated by the models. These models demonstrate that V_P/V_S measured at the surface is not that of the anomalous zone, but is related to it by a transfer function, involving the shape and velocity gradient of the zone boundary.*

Soviet seismologists (*1, 2*) found significant delays in P-wave arrival times relative to S-wave arrival times for foreshocks that preceded large earthquakes in the Garm region of the Soviet Union (*3*). These observations were confirmed in upstate New York and in southern and central California (*4*). They have been explained by dilatancy (*5*), and many related phenomena have been correlated as a basis for earthquake prediction (*6*). One aspect of the Soviet observations has not yet been dealt with quantitatively—the fact that the anomalous region is small compared to the dimensions of the seismic array. In this report we deal only with this problem of how a localized anomalous region can produce the distant effect.

The Russians discovered that travel times were anomalous only for small earthquakes occurring within a radius of 5 to 10 km of the focus of a subsequent large earthquake. This was revealed in "Wadati" diagrams (*7*) of these precursor shocks constructed by Semenov (*1*). We attacked the problem of whether a suitably small dilatant region can produce similar Wadati diagrams.

Dilatancy is believed to be due to microfractures created or enlarged as the stress increases in a rock before fracture (*8*). These cracks may be expected to have a preferred orientation, in which case V_P would vary with the direction of propagation. We use Garbin and Knopoff's analysis (*9*) of elastic wave propagation through a medium permeated by circular cracks which are small compared to the seismic wavelength. For cracks of random orientation

$$\left(\frac{V_P^0}{V_P}\right)^2 = 1 + \frac{Na^3}{v}\left(\frac{262}{105}\right) \quad (1)$$

where V_P^0 and V_P are the P-wave velocities in the uncracked and cracked regions, respectively, and N is the number of cracks of radius a in the volume v. For parallel cracks

$$\left(\frac{V_P^0}{V_P}\right)^2 = 1 + \frac{Na^3}{v}\left(\frac{2}{3} + \frac{40}{7}\cos^2\theta - \frac{8}{21}\cos^4\theta\right) \quad (2)$$

where θ is the angle between the geometric ray and the crack normal. For cracks with normals randomly distributed in a plane

$$\left(\frac{V_P^0}{V_P}\right)^2 = 1 + \frac{Na^3}{v}\left(\frac{2}{3} + \frac{20}{7}\cos^2\theta - \frac{1}{7}\cos^4\theta\right) \quad (3)$$

where θ is the angle from the ray to the plane normal. In a thrust fault region like Garm, one might expect the greatest (compressive) principal stress to be horizontal and the least to be vertical, leading to horizontal extension fractures. Hence, Eq. 2 would be appropriate, with θ measured from the horizontal (that is, V_P least in the vertical direction). In many thrust regions, however, the observed joints and microcracks are predominantly vertical, because of warping of the thrust near the surface (*10*). In this case Eq. 3 applies, with θ measured from the vertical (V_P least in the horizontal direction). All three cases are explored in our model. We assume that V_S remains unchanged; the propagation of S waves, which depends on polarization, is beyond the scope of the present study. In real materials V_S is also reduced by dilatancy, but much less than V_P. We believe that a particular V_P reduction in our model corresponds to a somewhat greater V_P reduction in nature.

The total volume of cracks is $v_c \simeq 3Na^3/A$, where A is the crack aspect ratio. In all cases, we assumed $Na^3/v =$

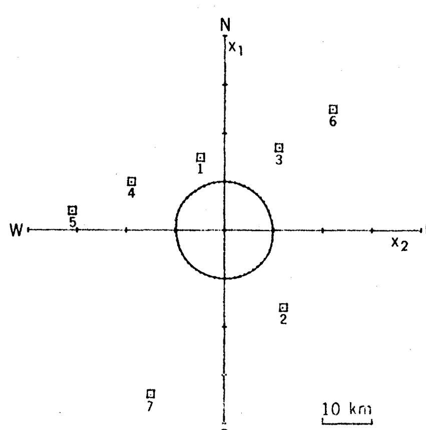

Fig. 1. Map of the seven seismic stations used by Semenov (*1*) in obtaining anomalous V_P/V_S values before large earthquakes near the center of the coordinate system. These stations are used in the models in this report, with an anomalous region centered on the origin. The circle of radius 10 km is the projection of models B and E (Fig. 2), and is approximately the size ascribed to the anomalous region by the Soviet scientists (*1, 2*).

Table 1. Data for Wadati plots in Fig. 3. Source locations are given relative to the center of the ellipsoid; axes are defined as follows: X_1, north; X_2, east; X_3, up. Values of V_P/V_S are means $\pm$ 1 standard deviation.

Plot in Fig. 3	Model	Coordinates of source location			V_P/V_S
		X_1 (km)	X_2 (km)	X_3 (km)	
A	Fig. 2A: Prolate, isotropic	0	0	−13	1.90 ± 0.02
B	Fig. 2B: Spherical, isotropic	2.5	0	−7	1.75 ± 0.05
C	Fig. 2F: Oblate, vertical cracks	3	0	−2	1.65 ± 0.03
D	Fig. 2G: Two spheres, isotropic with vertical cracks	−6	0	−1	1.63 ± 0.14
E	Fig. 2F: Oblate, vertical cracks	7	0	−2	1.60 ± 0.04
F	Fig. 2G: Two spheres, isotropic with vertical cracks	4.2	4.2	−1	1.55 ± 0.05

0.2, corresponding to an 18 percent reduction in V_P in the case of randomly oriented cracks; hence the volume increase $v_c/v = 0.6/A$. Measured aspect ratios of dilatant cracks are about 10^4 (*11*). This corresponds to a volumetric strain of 6×10^{-5}, or a linear expansion of 2 cm/km for randomly oriented cracks. The volume changes associated with dilatancy are important because they determine the local tilts accompanying premonitory dilatancy, whose measurement could constitute an important predictive technique.

The dilatant region is taken to be a spheroid, with its unique axis vertical, buried in a homogeneous half-space. The test of the model is a full three-dimensional calculation in which Wadati diagrams are constructed from the P and S arrival times at a real array of seismic stations. The foreshocks are presumed to originate at points throughout the assumed anomalous region. We call the result a V_P/V_S distribution function (VDF), since it constitutes a three-dimensional distribution of apparent V_P/V_S from sources throughout the anomalous region. The Wadati diagram is different for each focal point within the anomalous region. In the case of the Soviet seismic stations in the Garm region (Fig. 1), however, V_P/V_S determined from Wadati diagrams does not vary greatly with azimuth of the source. Hence, the behavior of the whole region can be portrayed by a single half-section of the VDF.

Figure 2 shows the VDF for sources within seven different types of anomalous regions: isotropic in Fig. 2, A to to C (Eq. 1), and anisotropic in Fig. 2, D to G (Eq. 3, vertical cracks). Anisotropy due to horizontal cracks does not yield sufficient reduction in V_P/V_S to be worthy of consideration. In all cases, the normal V_P/V_S is taken to be 1.75, a typical value for the Garm region. These cross sections were produced by computer programs for geometric ray tracing in three dimensions in an anisotropic medium. No reflected or diffracted waves were considered. They would be delayed relative to the direct wave and would thus enhance the apparent V_P/V_S anomaly.

The geometry of representation ellipsoids for Cartesian tensors is utilized (*12*). The anisotropy is approximated by a velocity ellipse (in agreement with Eqs. 1 to 3 to better than 1 percent). The problem then reduces to ray tracing from the assumed source location through the refracting boundary of the anomalous region to each of the receiving stations. This is done by conventional matrix methods. The only part of the solution that may be unfamiliar is the expression of Snell's law in matrix form

$$\frac{\epsilon_{ijk}N_jV_k^{(i)}}{V_n^{(i)}V_n^{(i)}} = \frac{\epsilon_{ijk}N_jV_k^{(e)}}{V_n^{(e)}V_n^{(e)}}$$

where ϵ_{ijk} is the alternating matrix, N_j is the normal to the boundary where the ray strikes it, and $V_i^{(i)}$ and $V_i^{(e)}$ are the wave-normal velocities of

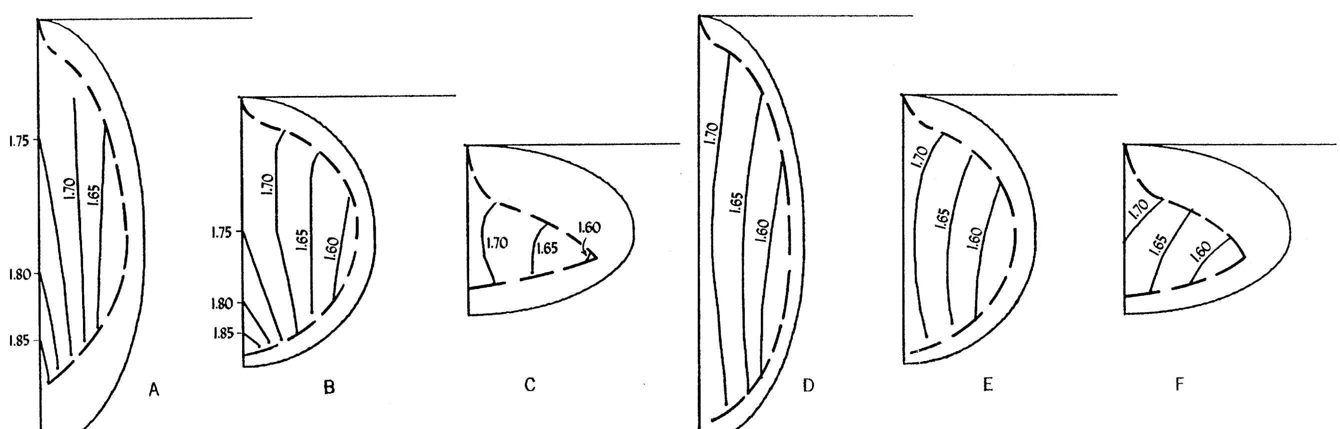

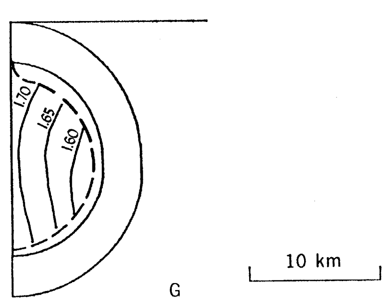

Fig. 2. Distribution plots for V_P/V_S within spheroidal anomalous regions. The spheroids are prolate (axis ratio $X_1/X_3 = 1/2$), spherical, and oblate ($X_1/X_3 = 2$), all tangent to the surface of the ground. In models A to F $Na^3/v = 0.2$ (Eqs. 1 to 3) and the volume of the source region and hence the number of cracks N is the same. (A to C) Source regions are isotropic and Eq. 1 is used. (D to F) Source regions have anisotropy due to vertical cracks and Eq. 3 is used. (G) Composite source region, the inner part anisotropic (Eq. 3) with $Na^3/v = 0.29$ and the outer one isotropic (Eq. 1) with $Na^3/v = 0.15$. Model G has the same total number of cracks and total volume, but the cracks are more concentrated near the center, as expected in nature. Sources located on the contour lines give the V_P/V_S values shown. The region outside the dashed line is a "shadow zone" where one or more of the seven stations fail to receive a first arrival (see text).

the incident and emergent waves. A search routine is employed to find the ray which goes to each station. When all seven stations are found, a least-squares fit is made to the data for $T_S - T_P$ against T_P; this line and the data points are plotted on a Wadati diagram.

This program has been extended to cover a multiregion anomalous zone, and the results of one such calculation are given in Fig. 2G. In principle, it is possible to do ray tracing by this method through any number of refracting boundaries of arbitrary shape and with arbitrary differences in anisotropy and velocity.

One has to be sure that the ray to the station is a true first arrival. In the case of the isotropic sphere, it is readily shown that no multipath can occur unless $V_P^0/V_P > 2^{1/2}$. A computer search indicates that no multipaths occur in any of the models presented here.

There is only a limited volume within the anomalous region from which these undiffracted, unreflected first arrivals may be observed at all seven stations. The boundary of this volume is indicated by the dashed lines in Fig. 2. Rays from sources outside the dashed line fail to reach one or more of the stations because of critical reflection. The apparent V_P/V_S is found to be unreliable when one or more stations are missed. The ratio may change as much as 0.2 when one station is missed, even with a tiny variation in source location. This is in contrast to very regular variation of V_P/V_S within the volume where all seven stations receive the first arrivals, although the variance of the data points may be large (for example, see Fig. 3D).

Figure 2 thus shows the VDF (within the seven-station volume) as contours of apparent V_P/V_S as a function of position of the source in the north-south vertical plane. It is seen that all models of Eqs. 1 and 3 have regions in which V_P/V_S is as low as the lowest value reported from Garm (1.62). The fraction of the anomalous volume which yields this low value is, however, greater in the anisotropic cases (Fig. 2, D to F). Moreover, the isotropic sphere and prolate ellipsoid (Fig. 2, A and B) contain volumes in which V_P/V_S is above normal (> 1.75).

Figure 2G shows that, as the cracks are concentrated toward the focus of the forthcoming earthquake, the radius at which a given reduction in V_P/V_S

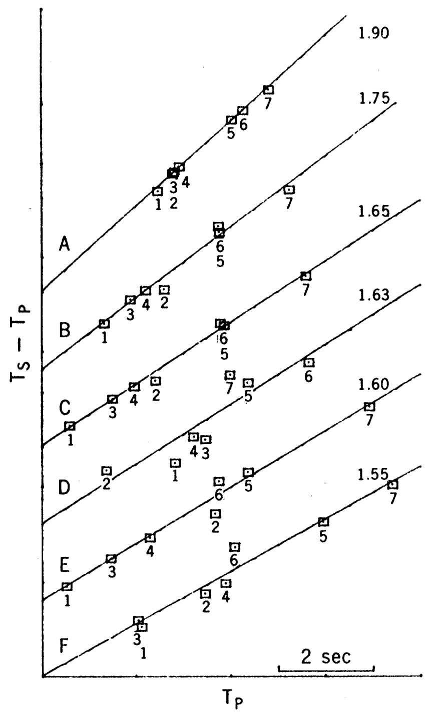

Fig. 3. Typical Wadati diagrams showing the range of variation of apparent V_P/V_S received at stations 1 to 7 (numbered points) from sources in models of Fig. 2. The model type, source location, and standard deviation of V_P/V_S for each plot are given in Table 1.

can be obtained is reduced (from ~ 9 to ~ 6 km). It should be noted that all models in Fig. 2 have the same total number of cracks. The difference between A, B, and C and D, E, and F is the anisotropy; the difference between E and G is the concentration toward the hypocenter.

In all the models illustrated in Fig. 2, sources nearer the center line yield higher V_P/V_S values than those farther out. A hint that this may be real is Semenov's illustration (*1*, figure 2, X and XIX) of some occurrences of relatively high V_P/V_S during the precursor period. These do not, however, approach the value of 1.85 which can occur in models A and B. The volume fraction in which V_P/V_S exceeds 1.75 is only 3 percent in A and 2 percent in B, so that abnormally high values of V_P/V_S would be expected to be a very rare occurrence if the anomalous zone resembled either A or B.

These models, simple as they are, yield surprisingly complex Wadati diagrams. Figure 3 shows a sample set, which displays variations from the highest V_P/V_S values (1.90) to the lowest (1.55). Table 1 gives the parameters of these events. When the source is on the center line of the ellipsoid, the points all fall on or nearly on a straight line (such as Fig. 3A). The maximum dispersion is shown in Fig. 3D ($V_P/V_S = 1.63 \pm 0.14$).

We find the Soviet observations, including the very small anomalous region, to be entirely consistent with the dilatancy theory. Anisotropy is not required to explain the observed Wadati diagrams. However, anisotropy is expected on physical grounds, and our results indicate that if anisotropy is present, the cracks must be predominantly vertical.

The most precise premonitory data, which led to an actual earthquake prediction, are those from Blue Mountain Lake, New York (*13*). The distribution of the seven stations in that study was unsuitable for testing the far-field effect. Quarry blast data show unambiguously that four of the stations were directly over the anomalous zone, one was above the boundary, and the other two were only slightly outside. The Blue Mountain Lake observations are well reproduced by our model by use of Eq. 1, with $Na^3/v = 0.2$ and an oblate spheroid with diameters 2 and 12 km whose top is 0.4 km below the surface. Specifically, the model reproduces the observed delay in arrival of quarry blast waves, the reduction in apparent V_P/V_S derived from foreshocks, and the decrease in apparent V_P/V_S with increasing depth of these foreshocks. It should be noted that the decrease of apparent V_P/V_S with depth requires no change in the intrinsic V_P/V_S in our model, but is a result of the different refraction of P and S waves. Moreover, the apparent V_P/V_S from the Wadati diagram is always substantially greater than that actually present in the anomalous zone.

These model studies show that surface seismic measurements do not, in general, reveal the actual seismic properties of the anomalous region. Inverting the surface data to find the nature of this region requires finding a transfer function which includes the effect of the shape and velocity gradient of the boundary of the region. The construction of more realistic models, including S-wave propagation and the paths of diffracted and reflected rays, should help in the solution to this problem.

DAVID T. GRIGGS*
DAVID D. JACKSON
LEON KNOPOFF
RONALD L. SHREVE
Institute of Geophysics and Planetary Physics, University of California, Los Angeles 90024

References and Notes

1. A. N. Semenov, *Phys. Solid Earth* **4**, 245 (1969).
2. M. A. Sadovsky, I. L. Nersesov, S. K. Nigmatullaev, L. A. Latynina, A. A. Lukk, A. N. Semenov, I. G. Simbireva, V. I. Ulomov, *Tectonophysics* **14**, 295 (1972).
3. The ratio V_P/V_S in an isotropic elastic medium is given by $(V_P/V_S)^2 = 2(1-\nu)/(1-2\nu)$, where ν is Poisson's ratio. In rocks V_P/V_S is typically in the range 1.55 to 1.85. We have arbitrarily selected $V_P = 5.5$ km/sec and $V_P/V_S = 1.75$ for the outer homogeneous half-space in our model.
4. Y. P. Aggarwal, L. R. Sykes, J. Armbruster, M. L. Sbar, *Nature (Lond.)* **241**, 101 (1973); J. H. Whitcomb, J. D. Garmany, D. L. Anderson, *Science* **180**, 632 (1973); R. Robinson, R. L. Wesson, W. L. Ellsworth, *ibid.* **184**, 1281 (1974).
5. A. Nur, *Bull. Seismol. Soc. Am.* **62**, 1217 (1972).
6. C. H. Scholz, L. R. Sykes, Y. P. Aggarwal, *Science* **181**, 803 (1973).
7. A Wadati diagram is a plot of the difference between the S and P wave arrival times $(T_S - T_P)$ versus the P wave arrival time (T_P) for all stations in the region which have clearly detected P and S arrivals. Although there were other stations in the region, only seven were used by Semenov (*1*) in constructing his Wadati diagrams. We therefore chose to use these seven stations in our model. In a homogeneous half-space, the slope of a Wadati diagram $[d(T_S - T_P)/dT_P]$ is equal to $(V_P/V_S) - 1$. What the Russians discovered was that this slope (and hence V_P/V_S) was dramatically reduced in the case of small earthquakes occurring a short time before a larger shock, and that this effect was only found for precursor earthquakes whose focus was within 5 to 10 km of the focus of the subsequent large shock, even though the most distant station was about 40 km from this focal point.
8. W. F. Brace, B. W. Paulding, Jr., C. H. Scholz, *J. Geophys. Res.* **71**, 3939 (1966).
9. H. D. Garbin and L. Knopoff, *Q. Appl. Math.* **30**, 453 (1973).
10. D. W. Stearns, in *Rock Mechanics Seminar*, R. E. Riecker, Ed. (Air Force Cambridge Research Laboratories, Cambridge, Mass., 1968), p. 97; D. W. Stearns and M. Friedman, *Am. Assoc. Pet. Geol. Mem.* **16**, 82 (1972).
11. G. Simmons, R. W. Siegfried, II, M. Feves, *J. Geophys. Res.*, in press.
12. J. F. Nye, *Physical Properties of Crystals* (Oxford Univ. Press, New York, 1957), p. 26.
13. Y. P. Aggarwal, L. R. Sykes, D. W. Simpson, P. G. Richards, *J. Geophys. Res.*, in press.

14. We acknowledge with pleasure stimulating conversations with M. A. Sadovsky, I. L. Nersesov, and S. K. Nigmatullaev. C. H. Scholz suggested to us earlier the possibility (which we then discounted) that displaced sources in a spherical isotropic anomalous region could produce the observed effect. Y. P. Aggarwal provided a preprint of an important paper (*13*) and critically reviewed our manuscript. J. W. McCormick gave valuable help in computer problems. One of us (D.T.G.) wishes to acknowledge the Hewlett-Packard Co. for creating a handy desk calculator which can easily manage these complex calculations. Supported by NSF grant GA-36077x. Publication No. 1373 of the Institute of Geophysics and Planetary Physics, University of California at Los Angeles.

* We regret that David T. Griggs died 31 December 1974 before seeing proofs for this report.

12 August 1974; revised 25 October 1974 ■

Folate Transport by the Choroid Plexus in vitro

Abstract. *Reduced folates are transported from blood into cerebrospinal fluid against a concentration gradient. In vitro, folates were transported into and released by isolated rabbit choroid plexuses. The choroid plexus uptake mechanism was specific for folates, energy dependent, and depressed by cold temperatures. In vivo, the choroid plexus may transport folates from blood to cerebrospinal fluid.*

Reduced folates, which are present at higher concentrations in brain and cerebrospinal fluid (CSF) than in plasma (*1*), play an essential role in brain metabolism (*2*). Yet, dihydrofolate reductase, the enzyme that catalyzes the reduction of folic acid (FA) to tetrahydrofolic acid (THF), is not present in mammalian brain (*3*). The high concentrations of reduced folates in CSF and brain are due to transport of reduced folates from blood—principally (+)L-5-methyltetrahydrofolate [(+)-MTHF] (*4*), which is the major folate in plasma (*5*). This transport system from blood is saturable; that is, increasing concentrations in plasma do not proportionately increase those in CSF (*6*). Levitt *et al.* suggested that a transport mechanism for reduced folates from blood into CSF through the blood-CSF barrier might reside in the choroid plexus (*4*). This study with the isolated choroid plexus shows that (i) there exists a specific, saturable, energy-dependent uptake system for folates in the choroid plexus; (ii) there also exists a mechanism for release of reduced folates from the choroid plexus; and (iii) the kinetic characteristics of this system of uptake and release are compatible with the choroid plexus being a locus of transport of reduced folates from blood to the CSF (*7*).

(±)[^{14}C]MTHF (60 mc/mmole) and [3′5′,9-^{3}H]FA (16 c/mmole) were obtained from Amersham/Searle. The naturally occurring stereoisomer [(+)L-[^{3}H]MTHF (0.17 c/mmole)] was biosynthesized by injecting a rat with 0.2 mc of [^{3}H]FA and isolating the (+)-[^{3}H]MTHF from the fresh liver the following day (*8*).

The choroid plexuses, obtained from brains of New Zealand white rabbits (1.5 to 2.0 kg) that were killed with intravenous pentobarbital (*9*), were individually placed in 3 ml of artificial CSF (*9*) containing [^{3}H]FA, or (±)-[^{14}C]- or (+)[^{3}H]MTHF. The artificial CSF also contained 1.0 m*M* thiourea and 2.0 m*M* sodium ascorbate to protect the reduced folates from oxidation (*4, 10*). The incubations were carried out in a metabolic shaker at 37°C under 95 percent O_2 and 5 percent CO_2 for 15 or 30 minutes. At the end of the incubation, each choroid plexus was wiped on a glass slide, weighed, and homogenized in 0.5 ml of H_2O. The radioactivity in tissue homogenates and media was determined, and the ratios of tissue to medium (T/M) were calculated (*9*). Substances added to the medium or conditions that depressed the ratios of [^{3}H]FA or (±)[^{14}C]MTHF are indicated in Table 1. Substances added to the medium or conditions that did not significantly affect the T/M ratio of (±)[^{14}C]MTHF included 0.17 μM methotrexate, 1.0 m*M* probenecid, 2.0 m*M* glutamic acid, 2.0 m*M* choline chloride, omission of glucose from the medium, or omission of glucose and incubation under 95 percent N_2 and 5 percent CO_2.

In order to establish whether altera-

Table 1. In virto uptake (expressed as T/M ratios) of [^{14}C]MTHF (left) or [^{3}H]FA (right) by rabbit choroid plexus. Choroid plexuses were incubated for 15 minutes unless otherwise indicated. Values are means ± standard error. The number of experiments at each point is indicated in parentheses.

Experimental condition	Uptake 15-minute (T/M)	MTHF control* (%)	Experimental condition	Uptake 15-minute (T/M)	FA control* (%)
Control, 80 n*M* (15)	11.9 ± 1.1		Control, 32 n*M* (3)	28.6 ± 1.7	
1°C (6)	0.6 ± 0.1	5	1°C (3)		
MTHF, 50.2 μM (3)	0.7 ± 0.1	6		0.5 ± 0.2	2
FA, 32.0 n*M* (3)	5.5 ± 0.4	46	FA, 0.91 μM (3)	2.9 ± 0.1	10
FA, 0.75 μM (3)	2.0 ± 0.3	17	FA, 61.0 μM (3)	2.0 ± 0.1	7
FA, 0.75 m*M* (3)	0.6 ± 0.1	5	MTHF, 0.10 μM (3)	5.5 ± 0.4	19
Dinitrophenol, 1 m*M*; iodoacetate, 2 m*M*; no glucose (12)	7.5 ± 0.7	63	Dinitrophenol, 1 m*M*; iodoacetate, 2 m*M*; no glucose (3)	9.2 ± 1.3	32
Methotrexate, 1.0 μM (3)	5.2 ± 0.6	44			
30-minute incubation, 80 n*M* (5)	26.3 ± 2.4	221	30-minute incubation, 32 n*M* (2)	55.1	193

* All the 15-minute percentage values indicated in the MTHF and FA columns differed significantly from their respective controls ($P < .05$) by Scheffe's method for multiple comparisons in the Gaussian analysis of variance (*13*).